Auger decay of $1\sigma_g$ and $1\sigma_u$ hole states of the N_2 molecule: Disentangling decay routes from coincidence measurements

S. K. Semenov,[1] M. S. Schöffler,[2] J. Titze,[2] N. Petridis,[2] T. Jahnke,[2] K. Cole,[2] L. Ph. H. Schmidt,[2] A. Czasch,[2] D. Akoury,[2,3] O. Jagutzki,[2] J. B. Williams,[4] T. Osipov,[3] S. Lee,[3] M. H. Prior,[3] A. Belkacem,[3] A. L. Landers,[4] H. Schmidt-Böcking,[2] Th. Weber,[3] N. A. Cherepkov,[1,2] and R. Dörner[2]

[1]*State University of Aerospace Instrumentation, 190000 St. Petersburg, Russia*

[2]*Institut für Kernphysik, University Frankfurt, Max-von-Laue-Strasse 1, D-60438 Frankfurt, Germany*

[3]*Lawrence Berkeley National Laboratory, Berkeley, California 94720, USA*

[4]*Department of Physics, Auburn University Auburn, Alabama 36849, USA*

(Received 25 February 2010; published 29 April 2010)

Results of the most sophisticated measurements in coincidence with the angular-resolved K-shell photoelectrons and Auger electrons and with two atomic ions produced by dissociation of N_2 molecule are analyzed. Detection of photoelectrons at certain angles makes it possible to separate the Auger decay processes of the $1\sigma_g$ and $1\sigma_u$ core-hole states. The Auger electron angular distributions for each of these hole states are measured as a function of the kinetic-energy release of two atomic ions and are compared with the corresponding theoretical angular distributions. From that comparison one can disentangle the contributions of different repulsive doubly charged molecular ion states to the Auger decay. Different kinetic-energy-release values are directly related to the different internuclear distances. In this way one can trace experimentally the behavior of the potential energy curves of dicationic final states inside the Frank-Condon region. Presentation of the Auger-electron angular distributions as a function of kinetic-energy release of two atomic ions opens a new dimension in the study of Auger decay.

DOI: 10.1103/PhysRevA.81.043426 PACS number(s): 33.80.Eh

I. INTRODUCTION

Auger-decay studies of molecules have a long history, though it seems that not all characteristics of that process have been investigated up to now. In atoms, the Auger decay corresponds to a transition between two (quasi)discrete states; therefore, the main attention in the atomic Auger-electron spectroscopy studies was focused on the identification of discrete lines [1,2]. The coincidence study of photoelectrons and Auger electrons enabled a much more detailed study of complex Auger-electron spectra with high precision [3–8]. As compared to atoms in diatomic molecules, due to lower symmetry (axial instead of spherical in the case of atoms) two new degrees of freedom appear: the vibrational and the rotational motion of nuclei. Due to that, the molecular Auger-electron spectra are substantially modified. The rotational splitting is too small to be resolved in the Auger-electron spectra, while the vibrational splitting is of the same order of magnitude as the Auger line widths and can broaden them. In addition to that, the photoionization followed by Auger decay produces a doubly charged molecular ion which often dissociates, creating atomic ions in their ground or excited states. In that way, the excitation energy of the initial state is distributed among the Auger electron, the nuclear motion, and the electronic excitation of the final products. Instead of a well-defined discrete line, a broad continuum of Auger-electron energies appears. This continuum cannot be identified by its energy position since usually several transitions are contributing at the same energy. Therefore, a basically new method is needed for studying the continuous Auger electron emission spectra in molecules. Such a method must take advantage of the axial symmetry of diatomic molecules in order to extract additional information not available in the standard Auger electron spectra. Namely, when the dissociation process is faster than the rotational motion, the latter can be disregarded, which opens the possibility to study the Auger decay of fixed-in-space molecules. That is the way to get the most detailed information about the Auger decay.

Let us consider the photoionization of the K shell of a N_2 molecule which produces a highly excited molecular-ion state. Within a short time of about 7 fs, this state decays, predominantly by emission of a fast Auger electron (around 360 eV). As a result, a doubly charged molecular ion is created with two holes in valence shells. At the next step this doubly charged molecular ion dissociates predominantly into two N^+ atomic ions with the kinetic-energy release (KER) in the region of 4 to 20 eV. The dissociation time is usually short compared with the molecular rotation; therefore, the direction of motion of the atomic ions gives the direction of the molecular axis at the time of photoabsorption and Auger decay.

The Auger decay of core ionized N_2 molecules has been studied using different methods, in particular, Auger-electron spectroscopy [9,10] and KER spectroscopy of the two N^+ ions [11–13]. In these studies, as in the case of atomic Auger decay, mainly the resonance structures were investigated. We report on the most detailed study of the Auger-decay process by detecting in coincidence the photoelectron, the Auger electron, and the two atomic singly charged ions (all of them being energy and angular resolved) using the cold target recoil ion momentum spectroscopy (COLTRIMS) technique [14,15]. The single-hole states in the K shell of a N_2 molecule are due to symmetry requirements split into two states, $1\sigma_g$ and $1\sigma_u$, and it is of interest to separate the Auger-decay processes of these two states. Their energy splitting is rather small, about 100 meV, which is nearly equal to the width of these states equal to 120 meV. Nevertheless,

recent very-high-resolution measurements made it possible to resolve these states in the photoelectron spectra [16,17], as well as in the Auger-electron spectra [18,19]. For the Auger-decay routes leading to dissociative states, the symmetry of an Auger electron cannot be deduced from its continuous energy alone; the initial singly ionized state has to be determined. That could in principal be done by measuring the Auger-electron energy and the KER with a resolution better than the g/u splitting. Alternatively, one can measure the photoelectron in coincidence to the Auger electron and deduce the character of the K hole from either the photoelectron energy or the emission angle. Since the necessary energy resolution is hard to achieve in a coincidence experiment, we have opted to use the photoelectron angle to tag the g or u core-hole state.

The angular distributions of photoelectrons from the K shell of a N_2 molecule have been studied theoretically, and from calculations it is known that at some angles predominantly the $1\sigma_g$ or $1\sigma_u$ shell is contributing [14,15]. By measuring the Auger-electron angular distribution in coincidence with the photoelectrons collected at these angles, one can separate the contributions of $1\sigma_g$ and $1\sigma_u$ shells to the Auger-decay process without need to resolve these transitions in energy [15]. As is shown in what follows, the corresponding Auger-electron angular distributions for transitions from the $1\sigma_g$ and $1\sigma_u$ hole states strongly depend on the configuration and the term of the final dicationic state. Comparing experimental and theoretical Auger-electron angular distributions, one can identify the transitions into different dicationic states. It is important to note that this method makes it possible to study mainly the continuous part of the Auger spectrum, which is hard to study by any other method [20,21]. This continuum is formed by Auger transitions into repulsive doubly charged molecular ion states, which do not create any resonance structure. However, the most intense resonant Auger transitions can also be studied by this method. The preliminary results of this study have been published in [22].

II. THEORY

A detailed description of the method used in our calculations is presented in [23–25]. Here we shall mention mainly the modifications introduced in the present calculations. We describe theoretically the angular distributions of photoelectrons from core levels and Auger electrons measured in coincidence with each other and in coincidence with the atomic ions resulting from the dissociation of a doubly charged molecular ion. The dissociation time is implied to be much shorter than the period of molecular rotation so that the direction of motion of dissociation products gives the direction of molecular axis at the time of the photoionization and the Auger decay. Since the dissociation step is not considered theoretically, we calculate the photoionization and the Auger decay of fixed-in-space molecules. We imply that a two-step model is applicable according to which the photon absorption is much faster than the Auger decay [1,2]. Under these conditions, the amplitude of the process can be presented as a product of a dipole d and a Coulomb V matrix elements:

$$f^{\lambda}_{f,i}(\vec{p}_A,\vec{p}) = \left\langle \Psi_f^{N-2}\psi^-_{\vec{p}_A}\middle|V\middle|\Psi_i^{N-1}\right\rangle\left\langle \Psi_i^{N-1}\psi^-_{\vec{p}}\middle|d_\lambda\middle|\Psi_0\right\rangle. \quad (1)$$

Here $|\Psi_0\rangle$ means the ground-state wave function of a molecule containing N electrons, λ is projection of a photon angular momentum in a photon frame with the z axis directed along the photon beam, Ψ_i^{N-1} and Ψ_f^{N-2} are a singly charged and a doubly charged molecular ion wave functions of the intermediate and final states, respectively, $\psi^-_{\vec{p}}$ and $\psi^-_{\vec{p}_A}$ are the photoelectron and the Auger-electron wave functions defined in the molecular frame, and $\vec{p}$ and $\vec{p}_A$ are the moments of the photoelectron and the Auger electron, respectively. In our case the intermediate state is the state with one hole in either the $1\sigma_g$ or the $1\sigma_u$ shell. The final state Ψ_f^{N-2} has two holes in the valence shells.

Doubly differential cross section for the process of core ionization of a N_2 molecule with a subsequent Auger decay in which both photoelectrons and Auger electrons are ejected at some fixed angles is given within the two-step model by the equation

$$\frac{d\sigma^{\lambda}_{fi}}{d\Omega_{p_A}d\Omega_p} \propto \left|f^{\lambda}_{fi}(\vec{p}_A,\vec{p})\right|^2, \quad i = 1\sigma_g \text{ or } 1\sigma_u. \quad (2)$$

Since the Lorentzian widths of the $1\sigma_g$ and $1\sigma_u$ photoelectron lines in N_2 are approximately equal to their energy splitting, in the Auger-electron–photoelectron coincidence experiment the photoelectrons from these shells cannot be energetically resolved [15]. This situation is described theoretically by treating the $1\sigma_g$ and $1\sigma_u$ states as if they were degenerate. Then instead of (2), we get

$$\frac{d\sigma_f}{d\Omega_{p_A}d\Omega_p} \propto \left|f_{f,1\sigma_g}(\vec{p}_A,\vec{p}) + f_{f,1\sigma_u}(\vec{p}_A,\vec{p})\right|^2. \quad (3)$$

Now we have a square modulus of the sum of two amplitudes which includes also the interference term, and this equation actually describes a deviation from the two-step model. The role of the interference term in Eq. (3) was discussed in [15,26].

In the present analysis we selected only the photoelectron ejection angles at which the predominant contribution is given by one of two K shells, that is, where one of the following conditions is fulfilled: $f_{f,1\sigma_g}(\vec{p}_A,\vec{p}) \ll f_{f,1\sigma_u}(\vec{p}_A,\vec{p})$ or $f_{f,1\sigma_g}(\vec{p}_A,\vec{p}) \gg f_{f,1\sigma_u}(\vec{p}_A,\vec{p})$. In these cases the interference term is small and to a good approximation can be neglected, so that only a square modulus of one of the two transitions in Eq. (3) gives a substantial contribution. Then all the general equations presented in [25] are valid here, too.

Our calculations have been performed in prolate spheroidal coordinates by the method described in [23]. The two steps (the photoionization and the Auger decay) are treated in the following way. At first the single-electron wave functions of the ground state of the neutral molecule are calculated in the Hartree-Fock (HF) approximation. After that, the wave functions for the intermediate singly charged molecular ion state are calculated in the relaxed core HF (RCHF) approximation as a solution of the HF equation with the potential formed by the self-consistent HF wave functions of a singly charged ion. The relaxed core approximation allows taking into account the rearrangement of the molecular orbitals to the creation of a core-hole state. However, the usual integer charge 1 for the ion core overestimates this effect; therefore, we proposed the modification of this method by using a fractional charge. The latter is selected empirically

from the condition to correctly describe the position in energy of the σ^* shape resonance of the photoionization cross section. For the K shell of N_2, the best agreement with experiment was found with the fractional charge equal to 0.7 [24]. The photoelectron wave function is calculated in the RCHF field and is orthogonalized to the ground-state wave functions. With the wave functions described previously, the dipole matrix elements are calculated according to Eqs. (10) and (11) of [25]. Many-electron correlations in the photoionization process are taken into account in the random-phase approximation by solving the corresponding equation for the dipole matrix elements presented in [23].

The initial state for the Auger decay is described by the same self-consistent RCHF wave functions, $\varphi_j^{(i)}$ of the singly charged molecular ion as in the photoionization step. For the doubly charged final molecular ion state, another set of the self-consistent HF wave functions $\varphi_j^{(f)}$ is calculated, this time with the integer charge 2. The Auger-electron wave function is calculated in the frozen field of the doubly charged ion. The Auger-decay amplitude is defined by the Coulomb matrix element given by Eqs. (34) and (40) of [25]. Since the wave functions $\varphi_j^{(i)}$ and $\varphi_j^{(f)}$ are not orthogonal, we calculate also the overlap matrix between the HF orbitals of the initial and final states $\mathbf{S}_{jk} = \langle \varphi_j^{(f)} | \varphi_k^{(i)} \rangle$ and obtain the Auger amplitude following the procedure proposed in [27]. The Auger-electron energy in the particular cases considered here is large, about 360 eV, so that the contribution of many-electron correlations is expected to be small. Therefore, we restricted calculations by the HF approximation as was done already in [25] for a CO molecule.

III. EXPERIMENT

The experiment was performed at beamline 11.0.2 of the Advanced Light Source of Lawrence Berkeley Laboratory via the COLTRIMS technique [28–31]. A supersonic gas jet, with a precooled nozzle provided an internally cold and well-localized target of N_2 molecules in their vibrational ground state. This gas jet was intersected by a beam of circularly polarized photons (419 eV) from beamline 11.0.2. The interception volume of well below 0.3 mm^3 was situated in a region of homogeneous parallel electric (12 V/cm) and magnetic (6.5 G) fields. The fields were prependicular to the gas jet. The fields guided the photoelectrons toward a multichannel plate detector (diameter 80 mm) with delay-line position readout [32]. The fields assured a 4π collection solid angle for the photoelectrons, while the fast Auger electrons where detected only within the small geometrical solid angle. They were used for calibration purposes only. In case the $N_2{}^{2+}$ ions break up, the resulted ionic fragments gain a large amount of kinetic energy from the Coulomb explosion. Therefore, the solid angle of detection depends on the orientation of the molecular axis at the instant of fragmentation: Those $N_2{}^{2+}$ ions that fragmented within 15° parallel to the electric field axis of our spectrometer were guided toward a second position-sensitive detector 72 cm from the interaction point. From the position of impact and the time of flight of the photoelectron and ions, we could determine their vector momenta, respectively. To improve the ion momentum resolution, we used a three-dimensional time and space-focusing ion optics setup (see Fig. 12 in [28]). Momentum vectors of the photoelectron and the two ions from the four-body final state were measured directly, whereas the momentum of the fourth particle, the Auger electron, was obtained through momentum conservation. This was possible only because the lens system avoided the deterioration of the ion momentum resolution due to the spatial extension of the interaction volume and since the N_2 jet was sufficiently cold in the direction of the gas beam due to cooling of the nozzle. For the nozzle conditions, great care was taken to avoid clustering of the beam while maintaining its narrow momentum spread.

The experiment yielded the full 4π solid angle distribution of the Auger electron and photoelectron and 1% solid angle for the ion momentum. We obtained an overall resolution of better than 50 meV (see Fig. 8) for the KER and 0.5 a.u. momentum resolution of the center-of-mass motion (i.e., the momentum of the Auger electron). The data were recorded in list mode, so any combination of angles and energies of the particles could be sorted out in the off-line analysis without repeating the experiment. The dataset used in the present analysis is the same as in [15,22]. All spectra reported were taken simultaneously with the same apparatus to reduce possible systematic errors.

IV. RESULTS

A. The basis of the method

Figure 1(a) shows the theoretical angular distribution of photoelectrons in the molecular frame ejected from the K shell of a N_2 molecule by circularly polarized light at photon energy 419 eV. This energy corresponds to the well-known σ^* shape resonance in the photoabsorption cross section [33] so that the photoelectron intensity at this photon energy has a maximum. The calculations have been performed with many electron correlations taken into account in the RPA approximation. It is seen that at the angles 60°–80° and 240°–260° the predominant contribution is given by the photoelectrons ejected from the $1\sigma_g$ shell. Vice versa, at the angles 140°–150° and 320°–330°, the predominant contribution is given by the $1\sigma_u$ shell. Therefore, to a good approximation one can say that by measuring the Auger electron angular distribution in coincidence with the photoelectrons collected at the angles mentioned previously, one can study the Auger-decay process separately for the $1\sigma_g$ and $1\sigma_u$ shells without need to resolve these transitions in energy [15]. In the experiment the photoelectrons were collected from a broader range of angles in order to increase the intensity of the signal. Namely, the angles 35°–85° and 215°–265° were used to select the contribution of the $1\sigma_g$ shell and the angles 115°–150° and 295°–330° for the contribution of the $1\sigma_u$ shell. As is evident from the figures, the separation of the contributions of the $1\sigma_g$ and $1\sigma_u$ shells is not complete, there is always some admixture of the state of the opposite parity which must be taken into account while comparing theory with experiment (see later in this article).

It is worth mentioning that absorption of circularly polarized light gives a better opportunity to separate the contributions of the $1\sigma_g$ and $1\sigma_u$ shells as compared to linearly polarized light. Figures 1(b) and 1(c) show the photoelectron

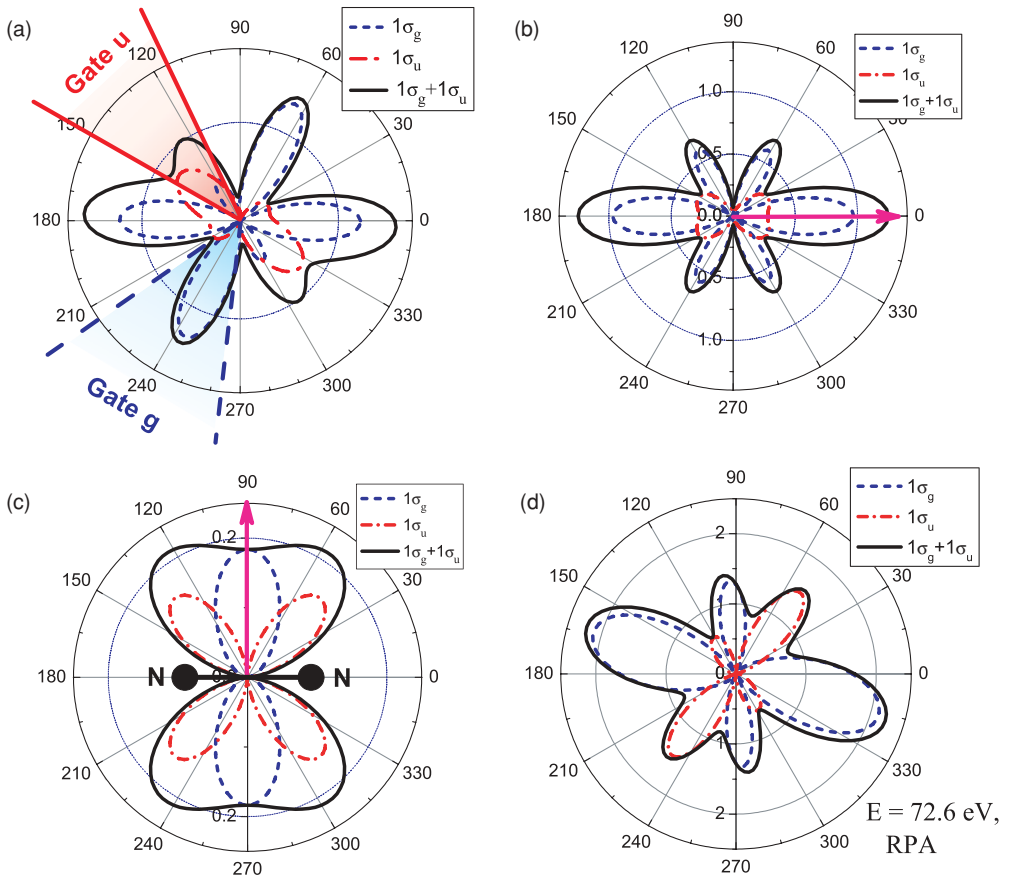

FIG. 1. (Color online) Molecular frame photoelectron angular distributions in the plane perpendicular to the photon beam calculated for several light polarizations and photon energies. (a) Left-handed circularly polarized light at photon energy 419 eV. (b) Light linearly polarized parallel to the molecular axis at 419 eV. (c) Light linearly polarized perpendicular to the molecular axis at 419 eV. (d) Left circular polarization at photon energy 483 eV. The molecular axis is directed along the horizontal axis, as is shown in panel (c). The contributions of $1\sigma_g$ and $1\sigma_u$ hole states are shown by dashed and dot-dashed lines, respectively. Their sum is shown by a solid line.

angular distributions for absorption of light linearly polarized parallel and perpendicular to the molecular axis, respectively, for the same photon energy 419 eV. In both cases one can easily separate the contribution of the $1\sigma_g$ shell, while the contribution of the $1\sigma_u$ shell greatly overlaps with the $1\sigma_g$ one and hardly can be separated. The other question is whether the particular photon energy can be favorable or unfavorable for such a separation, or an experiment can be performed at any photon energy. As an example, we show in Fig. 1(d) the photoelectron angular distribution for circularly polarized light at photon energy 483 eV (the photoelectron energy 73 eV). Here one can also quite well separate the contributions of the $1\sigma_g$ and $1\sigma_u$ shells. So the method can be applied at different photon energies and is not bound to the shape resonance.

To interpret the Auger electron spectra corresponding to the decay of the $1\sigma_g$ or $1\sigma_u$ hole state, we performed calculations of Auger-electron angular distributions for all possible final doubly charged molecular ion states with two holes in the outermost $3\sigma_g$,$1\pi_u$, or $2\sigma_u$ shells. Single configuration approximation was used in these calculations. These angular distributions strongly depend on the configuration and the term of the dicationic final state. Since in the experiment mainly the dissociating states are contributing, we concentrate on the consideration of these states. Figure 2 shows the potential energy curves for several states of the N_2^{2+} ion taken from Refs. [11,34–36]. As we already mentioned, the photoionization and the Auger decay processes are fast compared to the nuclear motion, and the internuclear distance during these processes remains weakly changed. Therefore, only the Franck-Condon (FC) region is contributing to the formation of doubly charged molecular ions. The vertical axis in Fig. 2 gives the KER energy of two N^+ ions after the dissociation process. The part of potential energy curves inside the FC region gives the range of KER energies to which the corresponding term is contributing.

Theoretical Auger electron angular distributions for several final dicationic states giving the predominant contribution to the Auger-electron intensity are presented in Fig. 3. Our calculations are in agreement with the earlier result of Ågren [37], according to which the triplet final states are giving rather small contribution to the Auger decay and can hardly be disentangled in our experiment; therefore, we do not show them. There is one exception, the $^3\Sigma_u$ term (see Fig. 2), which has a local minimum and for which the quasidiscrete final states are observed and identified as discussed later in this article. Similarly, there are quasidiscrete states corresponding to the $^1\Sigma_u$ term, which has a local minimum in the potential energy curve, too.

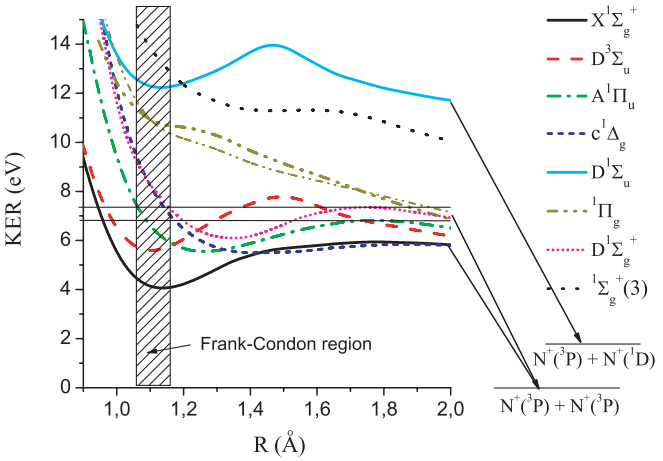

FIG. 2. (Color online) Potential energy curves from Refs. [11, 34–36] for several final dicationic states mentioned in the figure. The zero KER corresponds to the dissociation limit into the $N^+(^3P) + N^+(^3P)$ ion states. For the $^1\Pi_g$ final state, two curves are shown, one from Ref. [35] (thick dash-dot-dot curve) and the other from Ref. [36] (thin dash-dot-dot curve). The horizontal lines mark the positions of potential energy barriers for the $A^1\Pi_u$ and $D^1\Sigma_g^+$ terms.

Now we have enough information to start the analysis of the experimental results. Figure 4 shows the angular distributions of the Auger electrons for a photon energy 419 eV measured in coincidence with the photoelectrons ejected at the directions corresponding to ionization of either $1\sigma_g$ or $1\sigma_u$ shell in accord with Fig. 1(a). In this way, the Auger-decay processes of the $1\sigma_g$ and $1\sigma_u$ states are separated. They are shown separately in Figs. 4(a) and 4(b), respectively. The vertical axis in these figures corresponds to the KER energy. As a function of KER, one can single out three regions corresponding to KER energies 7–7.5 eV, 7.5–9.5 eV, and 10.3–11.5 eV, where the angular distributions have different characteristic features. Comparing theoretical and experimental angular distributions one can determine the main Auger-decay channels contributing at a given KER. Since the KER for any final state is defined by the internuclear distance at which the Auger decay takes place, the analysis of the KER dependence of the Auger-electron angular distributions makes it possible to determine the internuclear distances at which a given Auger-decay channel contributes. The separation of the Auger-decay processes of the $1\sigma_g$ and $1\sigma_u$ core holes plays the key role in this analysis.

B. Analysis of the coincidence Auger-electron–photoelectron spectra

Let us start from the KER energies 7–7.5 eV. From Fig. 2 follows that three final states are contributing here, $(3\sigma_g)^{-1}(1\pi_u^{-1})\ ^1\Pi_u$, $(1\pi_u)^{-2}\ ^1\Sigma_g^+$, and $(1\pi_u)^{-2}\ ^1\Delta_g$. Figure 5 shows the comparison of theoretical results with the experimental data (in arbitrary units). Since in theory the dissociation process is not considered, the theoretical angular distributions are not connected with any definite value of KER, while in experiment we have a contribution of a well-defined KER energy region. Therefore, the relative contributions of the three final states mentioned previously are taken theoretically as free parameters fitted by comparison with the experiment. The result of this fitting gives for the relative contributions of these states the following ratio: $I(^1\Pi_u) : I(^1\Sigma_g^+) : I(^1\Delta_g) = 1 : 0.7 : 0.7$. Figures 5(a) and 5(b) show the relative contributions of these transitions together with their sum. For the $1\sigma_g$ hole

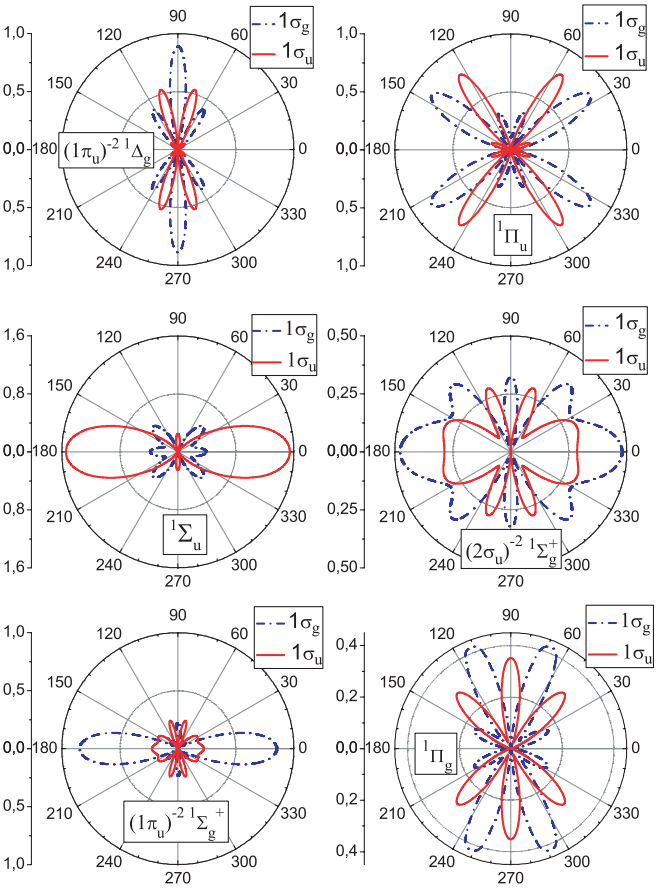

FIG. 3. (Color online) Theoretical Auger-electron angular distributions for several final dicationic states mentioned in the figures, giving the main contribution to the Auger-electron intensity. The molecular axis is directed along the horizontal axis.

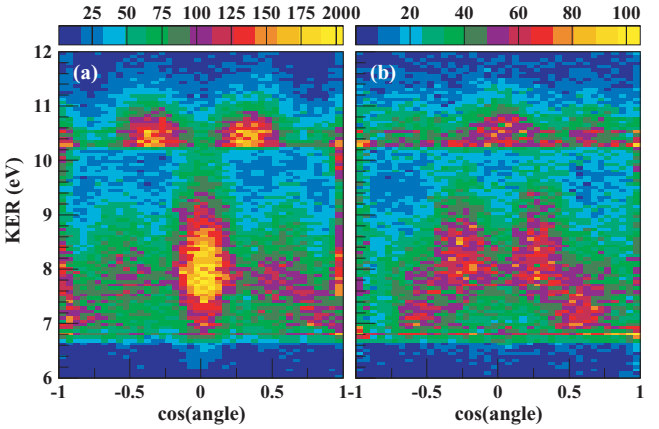

FIG. 4. (Color online) Experimental Auger-electron intensities measured as a function of cosine of the ejection angle θ relative to the molecular axis (horizontal axis) and of KER (vertical axis). Panels (a) and (b) correspond to the Auger decay of $1\sigma_g$ and $1\sigma_u$ hole states, respectively.

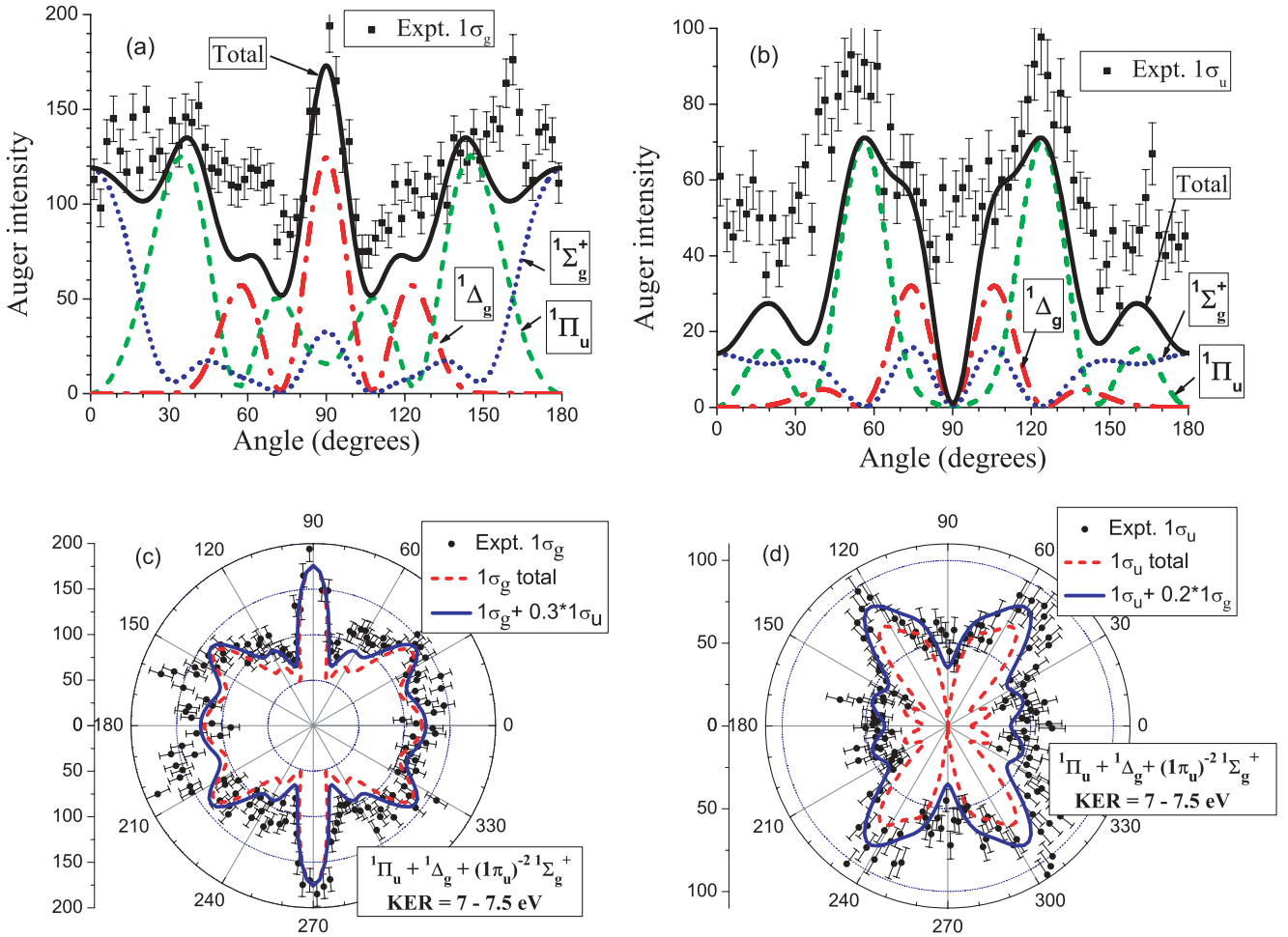

FIG. 5. (Color online) Auger electron angular distributions (in arbitrary units) measured in coincidence with photoelectrons (points with error bars) corresponding to ionization of either $1\sigma_g$ (a, c) or $1\sigma_u$ (b, d) shell, integrated over KER energies from 7 to 7.5 eV. Molecular axis is directed along the horizontal axis. The theoretical calculations (normalized to the experiment) include the Auger transitions to the following doubly charged molecular ion states $(3\sigma_g)^{-1}(1\pi_u)^{-1}\,{}^1\Pi_u$, $(1\pi_u)^{-2}\,{}^1\Delta_g$, and $(1\pi_u)^{-2}\,{}^1\Sigma_g^+$. The dashed and solid lines in (c) and (d) show the results of calculation without and with the inclusion of the admixture of the hole state of the opposite parity, correspondingly (see the text for detail).

state [Fig. 5(a)] the main maximum at 90° is given by the ${}^1\Delta_g$ term, the maxima at about 30° and 150° are due to the ${}^1\Pi_u$ term, and finally the only nonzero contribution at 0° and 180° is given by the ${}^1\Sigma_g^+$ term. For the $1\sigma_u$ hole state [Fig. 5(b)] the main maxima at 55° and 125° are defined by the ${}^1\Pi_u$ term, while the two maxima at 75° and 105° due to the ${}^1\Delta_g$ term make the main maxima broader. The only contribution at 0° and 180° is given again by the ${}^1\Sigma_g^+$ term. In Figs. 5(c) and 5(d) the total contributions from Figs. 5(a) and 5(b) are shown by dashed curves. The agreement between theory and experiment is satisfactory. Let us now take into account the fact that the separation of contributions of the $1\sigma_g$ and $1\sigma_u$ shells in the coincidence experiment is not complete, as is evident from Fig. 1(a). We must allow some admixture of the hole state of the opposite parity to each angular distribution. With such an admixture (added with a fitted parameter) the theoretical curves shown by solid lines in Figs. 5(c) and 5(d) are coming to a fairly good agreement with the experiment. The main lobes and their relative intensities are correctly reproduced by the theory.

Figure 6 shows the comparison of calculated and measured Auger-electron angular distributions at KER energies from 8 to 9 eV. In accord with Fig. 2 only two doubly charged molecular ion states $(1\pi_u)^{-2}\,{}^1\Delta_g$ and $(1\pi_u)^{-2}\,{}^1\Sigma_g^+$ are contributing here. The $(1\pi_u)^{-2}\,{}^1\Delta_g$ state is responsible for (i) the intensive lobe at the ejection angle 90° (above the horizontal axis) and two smaller lobes at 57.5° and 122.5° for the $1\sigma_g$ state, and (ii) the intensive lobes at the angles 75° and 105° for the $1\sigma_u$ state. The $(1\pi_u)^{-2}\,{}^1\Sigma_g^+$ state contributes mainly along the molecular axis at the angles 0° and 180° (qualitatively similar results though without resolving the contributions of $1\sigma_g$ and $1\sigma_u$ hole states have been obtained theoretically in [20]). Dashed lines again show the results obtained for pure $1\sigma_g$ or pure $1\sigma_u$ hole states. The relative contributions of different terms in the fitted curve is $I({}^1\Delta_g) : I({}^1\Sigma_g^+) = 1 : 0.87$. For the $1\sigma_u$ state agreement with experiment is only qualitative. However, after adding the contribution of the state of the opposite parity shown by solid lines in Fig. 6, the agreement with experiment is becoming quite satisfactory. The amount of admixture is defined by fitting to the experiment.

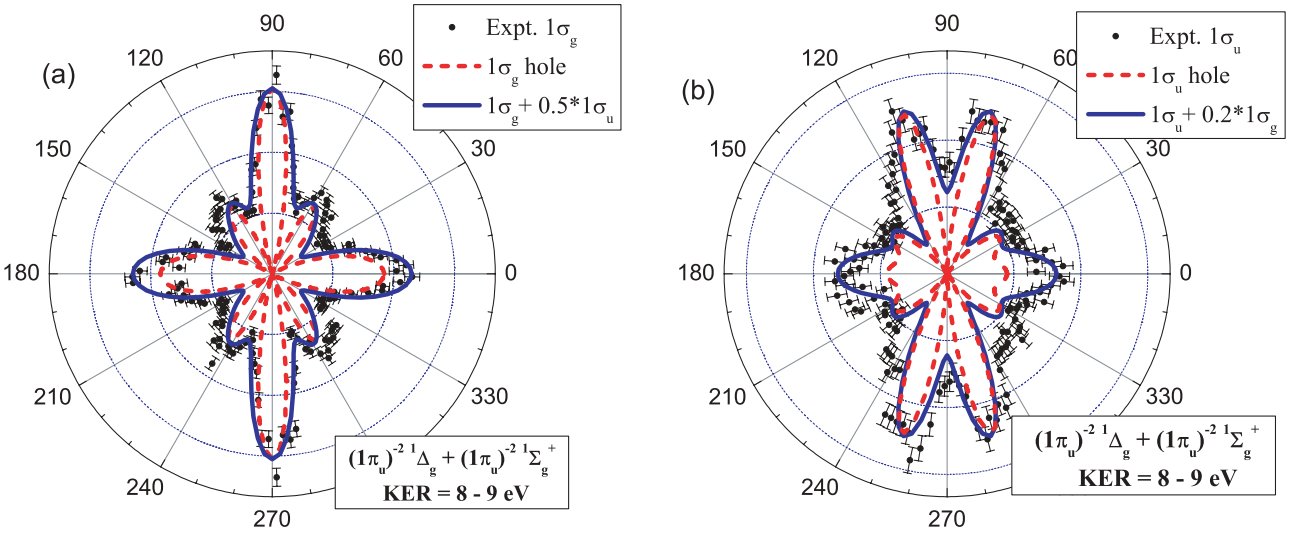

FIG. 6. (Color online) The same as in Figs. 5(c) and 5(d) for KER energies from 8 to 9 eV. Theoretical Auger transitions to the doubly charged molecular ion states $(1\pi_u)^{-2}\,{}^1\Delta_g$ and $(1\pi_u)^{-2}\,{}^1\Sigma_g^+$ are included.

Finally, at KER between 10.2 and 11 eV three terms are contributing to the angular distributions shown in Fig. 7, namely, $(2\sigma_u)^{-1}(1\pi_u)^{-1}\,{}^1\Pi_g$, ${}^1\Sigma_g^+(3)$ (see Fig. 2), and $(3\sigma_g)^{-1}(2\sigma_u)^{-1}\,{}^1\Sigma_u$. The last term is responsible for several discrete transitions appearing at these KERs. The characteristic features of these angular distributions are defined basically by the $(2\sigma_u)^{-1}(1\pi_u)^{-1}\,{}^1\Pi_g$ term. Namely, this term gives the main contribution at the angles 70° and 110° for the $1\sigma_g$ hole state and at 45°, 90°, and 135° for the $1\sigma_u$ hole state. As to the ${}^1\Sigma_g^+(3)$ state, from the calculations of Ågren [37] follows that though the main configuration contributing to this state is $(2\sigma_u)^{-2}$, the admixture of other configurations like $(1\pi_u)^{-2}$ is substantial. Since in our calculations the configuration interaction is not taken into account, we included into our fitting two separate configurations, $(2\sigma_u)^{-2}$ and $(1\pi_u)^{-2}$. The ratio of different theoretical contributions to the fitted curve is $I({}^1\Pi_g) : I({}^1\Sigma_g^+) : I({}^1\Sigma_u) = 1 : 0.2 : 0.12$. The results of fitting are again in reasonable agreement with the experiment.

The contributions of different triplet final states have not been identified in our fittings due to their small contribution, as we mentioned previously. The remaining difference between theory and experiment can be explained by approximations accepted in our calculations. In particular, the calculated Auger-electron angular distributions correspond to a fixed equilibrium internuclear distance, while in experiment the internuclear distance varies inside the FC region. Evidently, the Auger-electron angular distributions depend on the internuclear distance.

Another source of error is connected with the description of the doubly charged final ion state. We calculated the angular distributions for a well-defined configuration of the final states, while calculations of potential energy curves for N_2^{2+} demonstrated that configuration mixing plays an important role [34–37]. Fortunately, the main final states, giving the principal contribution to the Auger-electron spectra, namely $(3\sigma_g)^{-1}(1\pi_u)^{-1}\,{}^1\Pi_u$, $(1\pi_u)^{-2}\,{}^1\Sigma_g^+$, $(1\pi_u)^{-2}\,{}^1\Delta_g$, and

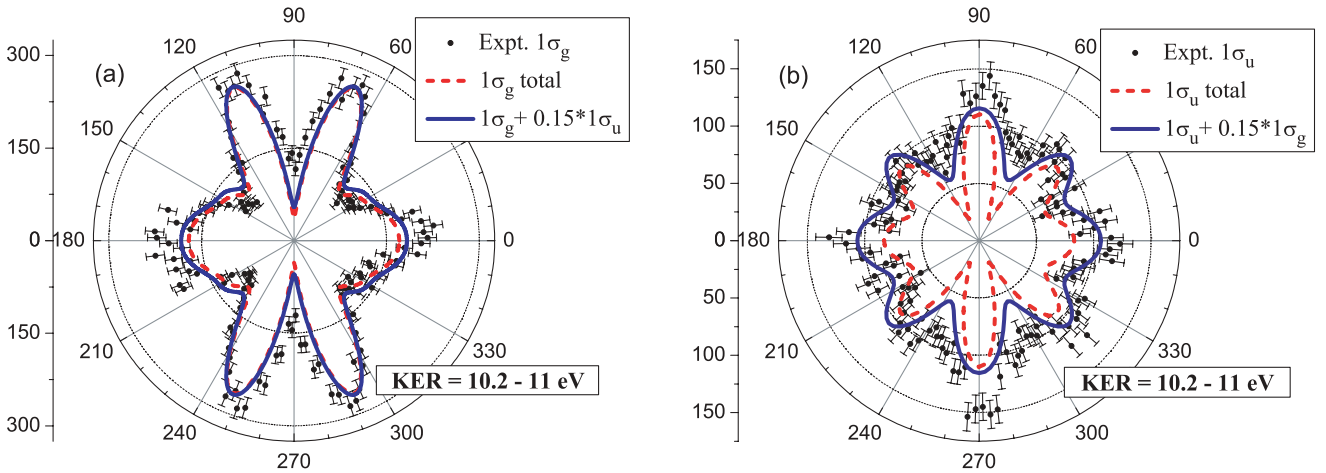

FIG. 7. (Color online) The same as in Figs. 5(c) and 5(d) for KER energies from 10.2 to 11 eV. Theoretical Auger transitions to the doubly charged molecular ion states $(2\sigma_u)^{-1}(1\pi_u)^{-1}\,{}^1\Pi_g$, $(1\pi_u)^{-2}\,{}^1\Sigma_g^+$, and $(3\sigma_g)^{-1}(2\sigma_u)^{-1}\,{}^1\Sigma_u$ are included.

$(2\sigma_u)^{-1}(1\pi_u)^{-1}\,{}^1\Pi_g$, can be represented sufficiently well by a single configuration [37].

When separating the contribution of the $1\sigma_u$ state at the angles 115°–150° and 295°–330°, it is evident from Fig. 1 that the contribution of the $1\sigma_g$ state is not negligible, so that the neglect of the interference term in Eq. (3) is not well justified. However, its inclusion makes the calculations much more laborious. One can mention also a possible contribution of many electron correlations beyond the HF approximation used in this article. It is difficult to give a numerical estimate of all these effects. Since the degree of agreement between theory and experiment in Figs. 5–7 is quite satisfactory, all possible theoretical improvements mentioned previously hardly can change the principal conclusions.

C. Discussion of KER spectrum

Figure 8 shows the total KER spectrum for all Auger-decay channels (that is without coincidence with photoelectrons and integrated over the angle θ relative to the molecular axis). This spectrum contains several strong discrete lines and a continuous contribution. Qualitatively, this spectrum is similar to the KER spectrum observed in [11] by electron scattering. According to the results demonstrated previously, a broad maximum between 7 and 10 eV is mainly formed by the transition to the $(1\pi_u)^{-2}\,{}^1\Delta_g$ state. It coincides with the region where the corresponding potential energy curve crosses the Frank-Condon region (see Fig. 2). To trace the contribution of this final state more precisely, we selected from the data shown in Fig. 4 the angles corresponding to the Auger electron emission perpendicular to the molecular axis (85°–95°). The corresponding results are shown in Figs. 9(c)and 9(e) for the $1\sigma_g$ and $1\sigma_u$ hole states separately and in Fig. 9(a) for the sum of these two states. As is evident from theoretical angular distributions shown in Fig. 3, for the $1\sigma_g$ hole state, practically only one ${}^1\Delta_g$ term contributes in this direction. According to Fig. 9(c), this contribution as a function of KER at first increases and then decreases inside the FC region, which is in

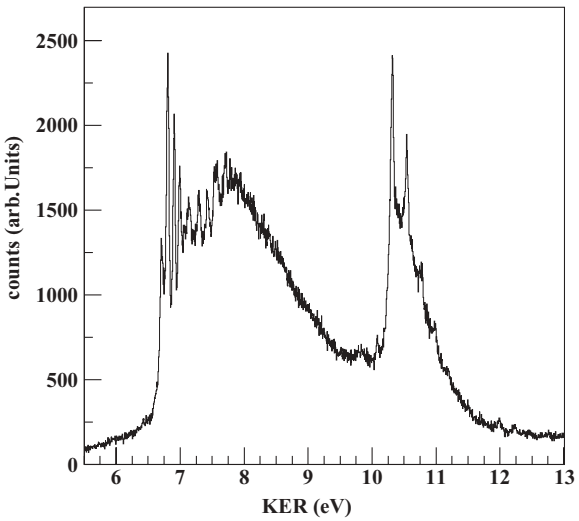

FIG. 8. Total experimental Auger-electron KER spectrum (in arbitrary units), which is the sum of contributions of the $1\sigma_g$ and $1\sigma_u$ states integrated over all Auger-electron emission angles.

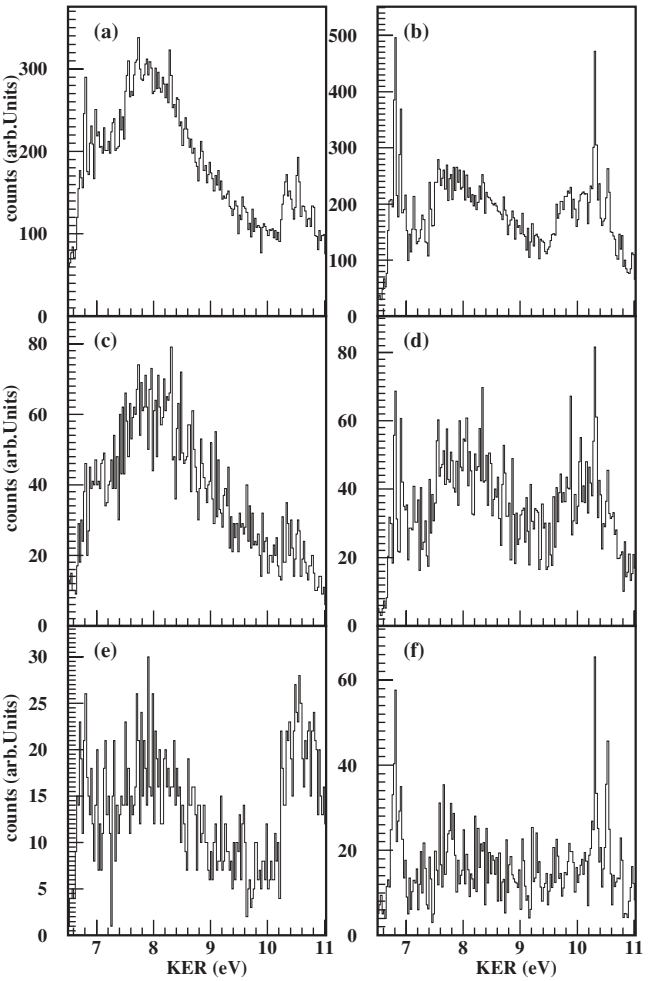

FIG. 9. Auger-electron intensities integrated over the angles $90° \pm 5°$, that is perpendicular to the molecular axis [(a), (c), and (e), left column], and over the angles $0° \pm 5°$ plus $180° \pm 5°$, that is parallel to the molecular axis [(b), (d), and (f), right column]. Top line, without separation of the contributions of the $1\sigma_g$ and $1\sigma_u$ hole states [(a) and (b)]; middle line, contribution of only $1\sigma_g$ hole state [(c) and (d)]; bottom line, contribution of only $1\sigma_u$ hole state [(e) and (f)].

accord with the behavior of the zero-order vibrational wave function of the ground state of N_2.

In the KER energy region between 6.8 and 7.5 eV a substantial contribution in Fig. 8 is given also by the transition to the $(3\sigma_g)^{-1}(1\pi_u)^{-1}\,{}^1\Pi_u$ final state. This is in agreement with the position of the corresponding potential energy curve inside the FC region in Fig. 4. It is important to mention that due to the potential barrier (at the internuclear distance about 1.8 Å) the contribution of this state inside the FC region is visible only at internuclear distances smaller than 1.1 Å. Due to that, its contribution has a sudden jump at a KER of 6.8 eV; at lower KER energies, the fast dissociation is not possible. This sudden jump is a characteristic feature of the KER spectrum in Fig. 8. Finally, the maximum between 10.3 and 12 eV is formed mainly by the $(2\sigma_u)^{-1}(1\pi_u)^{-1}\,{}^1\Pi_g$ state. This contribution is also seen in Fig. 9(e), where there is a sharp increase of intensity starting from 10.3 eV. This is in accord with the behavior of the theoretical Auger-electron angular distribution for the ${}^1\Pi_g$ term for the $1\sigma_g$ hole state

which has a maximum at the angle 90° (see Fig. 3). There are two calculations of the potential energy curve for this state shown in Fig. 2 which do not coincide well within the FC region. The sharp increase of the Auger-electron intensity as KER of 10.3 eV definitely testifies to the presence of some potential barrier like in the case of the $^1\Pi_u$ final state, or at least to a nonmonotonic decrease of the potential energy curve with increasing internuclear distance like in the calculations of Taylor [35]. However, in the latter case the position of the potential energy curve inside the FC region does not fit the position of the maximum in the experimental KER spectrum. Therefore, we conclude that the potential energy curve for the $^1\Pi_g$ dicationic state needs to be calculated more accurately.

The contribution of the $(1\pi_u)^{-2}\,{}^1\Sigma_g^+$ state does not produce a well separated maximum in the total KER spectrum shown in Fig. 8. To separate the contribution of Σ states, we show in Figs. 9(b), 9(d), and 9(f) the parts of the spectrum of Fig. 4 in the direction of the molecular axis, that is, in the regions −5° to +5° and 175°–185°. For the $1\sigma_g$ hole state in Fig. 9(d) there are two broad maxima in the Auger-electron intensity along the molecular axis, which must be connected with the Σ terms (Π and Δ terms do not contribute along the molecular axis). The first of these maxima corresponds to the $(1\pi_u)^{-2}\,{}^1\Sigma_g^+$ state, which is in agreement with the behavior of the corresponding potential energy curve shown in Fig. 2. The second maximum is most probably produced by the $^1\Sigma_g^+(3)$ state also shown in Fig. 2 which is connected mainly with the $(2\sigma_u)^{-2}$ configuration. Its position in Fig. 2 is shifted upward by about 4 eV compared to other potential energy curves contributing at KER energies studied by us, which means that the corresponding state dissociates into the pair of excited atomic ions $N^+(^1D)+N^+(^1D)$ or into $N^+(^3P)+N^+(^1S)$.

From the analysis of the Auger-electron angular distributions presented in Fig. 4 we can conclude that a strong discrete transition at KER of 6.8 eV corresponds to the $(2\sigma_u)^{-1}(3\sigma_g)^{-1}\,{}^3\Sigma_u$ state. Two other strong discrete transitions at KERs of 10.32 and 10.54 eV can be unambiguously indentified as transitions to the $(2\sigma_u)^{-1}(3\sigma_g)^{-1}\,{}^1\Sigma_u^+$ state, which is in agreement with the identification made earlier by Lundqvist *et al.* [11]. This is supported by the presence of contribution of these lines along the molecular axis in Figs. 9(d) and 9(f) for both $1\sigma_g$ and $1\sigma_u$ shells, in accord with the corresponding theoretical angular distributions shown in Fig. 3.

V. CONCLUSIONS

We demonstrated that the measurement in coincidence of photoelectrons and Auger electrons together with the singly charged atomic ions produced by dissociation of doubly charged molecular ion makes it possible to separate Auger-decay channels corresponding to the $1\sigma_g$ and $1\sigma_u$ hole states of N_2 without the need to separate these transitions in energy. In addition, it becomes possible to disentangle the contributions of different repulsive doubly charged molecular ion states as a function of KER energy by comparing corresponding theoretical Auger-electron angular distributions in the molecule fixed frame. This makes it possible to follow experimentally the behavior of the potential energy curves for dicationic final states within the Frank-Condon region. Presentation of the Auger-electron angular distributions as a function of KER of two atomic ions opens an additional dimension in the study of Auger decay. In particular, one can follow the contribution of a given Auger transition as a function of internuclear distance. The strongest discrete lines can also be identified by this method. The method can be used at different photon energies and with different light polarization, though circularly polarized light seems to give a better resolution of contributions of the $1\sigma_g$ and $1\sigma_u$ hole states. Evidently, this method is applicable to other homonuclear diatomic molecules.

ACKNOWLEDGMENTS

We acknowledge outstanding support by the staff of the Advanced Lights Source, in particular by Hendrik Bluhm and Tolek Tyliszczak. The work was supported by the Deutsche Forschungsgemeinschaft and by the office of Basic Energy Sciences, Division of Chemical Sciences of the US Department of Energy, under Contract Nos. DE-AC03-76SF00098 and DE-FG02-07ER46357. N.A.C. acknowledges the financial support of Deutsche Forschungsgemeinschaft through a Mercator professorship. S.K.S. and N.A.C. acknowledge the hospitality of Goethe University in Frankfurt am Main and the financial support of RFBR (Grant No. 09-03-00781-a).

[1] T. Åberg and G. Howat, in *Encyclopedia of Physics*, edited by S. Flügge and W. Mehlhorn (Springer-Verlag, Berlin, 1982), Vol. 31, p. 469.

[2] H. Aksela, S. Aksela, and N. M. Kabachnik, in *VUV and Soft X-Ray Photoionization Studies*, edited by U. Becker and D. A. Shirley (Plenum, New York, 1996), p. 401.

[3] H. W. Haak, G. A. Sawatzky, and T. D. Thomas, Phys. Rev. Lett. **41**, 1825 (1978).

[4] E. von Raven, M. Meyer, M. Pahle, and B. Sonntag, J. Electron Spectrosc. Relat. Phenom. **52**, 677 (1990).

[5] B. Kämmerling and V. Schmidt, Phys. Rev. Lett. **67**, 1848 (1991); **69**, 1145 (1992).

[6] N. M. Kabachnik, J. Phys. B **25**, L389 (1992).

[7] P. Bolognesi, A. De Fanis, M. Coreno, and L. Avaldi, Phys. Rev. A **70**, 022701 (2004); **72**, 069903(E) (2005).

[8] F. Da Pieve, S. Di Matteo, D. Sebilleau, R. Gunnella, G. Stefani, and C. R. Natoli, Phys. Rev. A **75**, 052704 (2007).

[9] W. E. Moddeman, T. A. Carlson, M. O. Krause, B. P. Pullen, W. E. Bull, and G. K. Schweitzer, J. Chem. Phys. **55**, 2317 (1971).

[10] W. Eberhardt, E. W. Plummer, I.-W. Lyo, R. Carr, and W. K. Ford, Phys. Rev. Lett. **58**, 207 (1987).

[11] M. Lundqvist, D. Edvardsson, P. Baltzer, and B. Wannberg, J. Phys. B **29**, 1489 (1996).

[12] N. Saito and I. Suzuki, J. Phys. B **20**, L785 (1987).

[13] M. J. Besnard, L. Hellner, G. Dujardin, and D. Winkoun, J. Chem. Phys. **88**, 1732 (1988).

[14] T. Jahnke *et al.*, Phys. Rev. Lett. **88**, 073002 (2002).

[15] M. S. Schöffler *et al.*, Science **320**, 920 (2008).

[16] U. Hergenhahn, O. Kugeler, A. Rüdel, E. E. Rennie, and A. M. Bradshow, J. Phys. Chem. A **105**, 5704 (2001).
[17] S. K. Semenov, N. A. Cherepkov, M. Matsumoto, K. Fujiwara, K. Ueda, E. Kukk, F. Tahara, T. Sunami, H. Yoshida, T. Tanaka, K. Nakagawa, M. Kitajima, H. Tanaka, and A. De Fanis, J. Phys. B **39**, 375 (2006).
[18] S. L. Sorensen, C. Miron, R. Feifel, M.-N. Piancastelli, O. Björheholm, and S. Svensson, Chem. Phys. Lett. **456**, 1 (2008).
[19] R. Püttner, H. Fukuzawa, X.-J. Liu, S. K. Semenov, N. A. Cherepkov, T. Tanaka, M. Hoshino, H. Tanaka, and K. Ueda, J. Phys. B **41**, 141001 (2008).
[20] Q. Zheng, A. K. Edwards, R. M. Wood, and M. A. Mangan, Phys. Rev. A **52**, 3940 (1995); A. K. Edwards, Q. Zheng, R. M. Wood, and M. A. Mangan, *ibid.* **55**, 4269 (1997).
[21] M. Ahmad, P. Lablanquie, F. Penent, J. G. Lambourne, R. I. Hall, and J. H. D. Eland, J. Phys. B **39**, 3599 (2006).
[22] N. A. Cherepkov *et al.*, Phys. Rev. A **80**, 051404(R) (2009).
[23] S. K. Semenov, N. A. Cherepkov, G. H. Fecher, and G. Schönhense, Phys. Rev. A **61**, 032704 (2000).
[24] S. K. Semenov, N. A. Cherepkov, T. Jahnke, and R. Dörner, J. Phys. B **37**, 1331 (2004).
[25] S. K. Semenov, V. V. Kuznetsov, N. A. Cherepkov, P. Bolognesi, V. Feyer, A. Lahmam-Bennani, M. E. Staicu Casagrande, and L. Avaldi, Phys. Rev. A **75**, 032707 (2007).
[26] N. A. Cherepkov, S. K. Semenov, and R. Dörner, J. Phys. Conf. Ser. **141**, 012001 (2008).
[27] K. Zähringer, H.-D. Meyer, and L. S. Cederbaum, Phys. Rev. A **45**, 318 (1992); **46**, 5643 (1992).
[28] R. Dörner, V. Mergel, O. Jagutzki, L. Spielberger, J. Ullrich, R. Moshammer, and H. Schmidt-Böcking, Phys. Rep. **330**, 95 (2000).
[29] J. Ullrich, R. Moshammer, A. Dorn, R. Dörner, L. Ph. H. Schmidt, and H. Schmidt-Böcking, Rep. Prog. Phys. **66**, 1463 (2003).
[30] T. Jahnke, Th. Weber, T. Osipov, A. L. Landers, O. Jagutzki, L. Ph. H. Schmidt, C. L. Cocke, M. H. Prior, H. Schmidt-Böcking, and R. Dörner, J. Electron Spectrosc. Relat. Phenom. **141**, 229 (2004).
[31] Th. Weber *et al.*, J. Phys. B **34**, 3669 (2001).
[32] O. Jagutzki, V. Mergel, K. Ullmann-Pfleger, L. Spielberger, U. Spillmann, R. Dörner, and H. Schmidt-Böcking, Nucl. Instrum. Methods A **477**, 244 (2002).
[33] J. L. Dehmer and D. Dill, Phys. Rev. Lett. **35**, 213 (1975).
[34] E. W. Thulstrup and A. Andersen, J. Phys. B **8**, 965 (1975).
[35] P. R. Taylor, Mol. Phys. **49**, 1297 (1983).
[36] R. W. Wetmore and R. K. Boyd, J. Phys. Chem. **90**, 5540 (1986).
[37] H. Ågren, J. Chem. Phys. **75**, 1267 (1981).